Co-registration and residual correction of digital elevation models: A comparative study

Tao Li[1,2], Yuanlin Hu[1,3], Bin Liu[4], Liming Jiang[1,2], Hansheng Wang[1], Xiang Shen[1]

[1]State Key Laboratory of Geodesy and Earth's Dynamics, Innovation Academy for Precision Measurement Science and Technology, Chinese Academy of Sciences, Wuhan, Hubei, 430077, China.
[2]University of Chinese Academy of Sciences, Beijing 100049, China.
[3]School of Geography and Information Engineering, China University of Geosciences, Wuhan, Hubei, 430074, China.
[4]State Key Laboratory of Remote Sensing Science, Aerospace Information Research Institute, Chinese Academy of Sciences, Beijing 100101, China.

Correspondence to: Xiang Shen (shen@apm.ac.cn)

Abstract

Digital elevation models (DEMs) are currently one of the most widely used data sources in glacier thickness change research, due to the high spatial resolution and continuous coverage. However, raw DEM data are often misaligned with each other, due to georeferencing errors, and a co-registration procedure is required before DEM differencing. In this paper, we present a comparative analysis of the two classical co-registration methods proposed by Nuth and Kääb (2011) and Rosenholm and Torlegard (1988). The former is currently the most commonly used method in glacial studies, while the latter is a seminal work in the photogrammetric field that has not been extensively investigated by the cryosphere community. Furthermore, we also present a new residual correction method using a generalized additive model (GAM) to eliminate the remaining systematic errors in DEM co-registration results. The performance of the two DEM co-registration methods and three residual correction algorithms (the GAM-based method together with two parametric-model-based methods) was evaluated using ~~23 Advanced Spaceborne Thermal Emission and Reflection Radiometer (ASTER) DEM pairs from the western margin of the Greenland Ice Sheet.~~multiple DEM pairs from Ice Sheet and mountain glaciers, including Advanced Spaceborne Thermal Emission and Reflection Radiometer (ASTER) DEMs, ZiYuan-3 (ZY-3) DEMs, Shuttle Radar Topography Mission (SRTM) DEMs, and Copernicus DEMs. The experimental results confirm our theoretical analysis of the two co-registration methods. The method of Rosenholm and Torlegard has a greater ability to remove DEM misalignments (~~4.6% on average and 15.3% maximum~~83.3% maximum) because it models the translation, scale, and rotation-induced biases, while the method of Nuth and Kääb considers translation only. The proposed GAM-based method performs statistically better than the two residual correction methods based on parametric regression models (high-order polynomials and the sum of the sinusoidal functions). A visual inspection reveals that the GAM-based method, as a non-parametric regression technique, can capture complex systematic errors in the DEM co-registration residuals.

1. Introduction

Differencing between multi-temporal digital elevation models (DEMs) is a widely used approach for mapping glacier elevation changes at local and regional scales (Bolch et al., 2011; Lin et al., 2017; Liu et al., 2019; Ke et al., 2022) (Bolch et al., 2011; Gardelle et al., 2013; Pieczonka et al., 2013; Liu et al., 2019). However, limited by the imaging and georeferencing techniques, systematic errors often exist in the raw DEMs (Rodriguez et al., 2006; Leprince et al., 2007) (Rodriguez et al., 2006), which can lead to wrong estimation of glacier mass change and false detection of glacier surges (Nuth and Kääb, 2011). Numerous studies have confirmed that a co-registration process is required to remove these biases before DEM differencing is conducted (Van Niel et al., 2008; Nuth and Kääb, 2011; Paul et al., 2015).

DEM co-registration has been extensively studied, and the existing methods can be broadly classified into two main categories. The first category requires an explicit data matching process (i.e., correspondence search). Typical methods in this category include: feature point based methods, e.g., the scale-invariant feature transform (SIFT) descriptor (Aguilar et al., 2012; Sedaghat and Naeini, 2018) and the method based on centroids of subwatersheds (Li et al., 2017); feature line based methods, e.g., methods based on stream networks or watershed boundaries (Karkee et al., 2008); the multi-feature based surface matching method (Wu et al., 2013); the iterative closest point (ICP) algorithm and its variants (Besl and Mckay, 1992; Rusinkiewicz and Levoy, 2001; Di et al., 2012); and the least squares 3D surface matching (LS3D) algorithm (Gruen and Akca, 2005; Akca, 2010). All of the above methods originate from image or point cloud processing studies, and they can be used for the coarse co-registration of DEMs without georeferenced information. However, the main disadvantage of these methods is that the correspondence finding procedure is very time-consuming when processing large DEMs. Moreover, the accuracy of the image-based methods (e.g., SIFT) is strongly dependent on extracting a large number of high-quality features, which is not an easy task for DEMs lacking sufficient textures.

The second category of DEM co-registration methods does not require an explicit matching process. The optimization objective of these methods is usually to minimize the sum of the vertical distances between two DEMs, where each pixel in the slavesecondary DEM implicitly corresponds to the same planimetric position in the masterreference DEM. These methods are not suitable for scenarios images lacking georeferenced information, but they are strongly recommended for high-accuracy applications where the DEMs have been georeferenced or coarsely co-registered. The typical algorithms in this category include grid search methods (Hofton et al., 2006; Rodriguez et al., 2006; Berthier et al., 2007; Van Niel et al., 2008; Cucchiaro et al., 2020) and terrain information based methods (Gorokhovich and Voustianiouk, 2006; Peduzzi et al., 2010; Nuth and Kääb, 2011). The grid search methods search for the best alignment result by stepwise shifting the slavesecondary DEM in a predefined window (e.g., 5 × 5 pixels). However, these methods have been rarely used in the recent literature because their brute-force search process comes with a huge computational cost. The terrain information based methods are derived from the analytical relationship between the elevation differences of the DEMs and terrain-related information. The method proposed by Nuth and Kääb (2011) employs the terrain slope and aspect as explanatory variables in the regression model, and is currently the most commonly used DEM co-registration algorithm in glacial studies (Vacaflor et al., 2022). In a much earlier study, Rosenholm and Torlegard (1988) developed an absolute orientation algorithm for stereo models based on terrain gradients. This method has been widely used for DEM co-registration in the photogrammetry field, but, unfortunately, has rarely been considered in the cryosphere community. To the best of our knowledge, only Noh and Howat (2014) adopted a similar approach to measure glacier elevation changes. However, the regression equation they used has a very complicated form because small-angle approximation is not used, and the algorithm is not easy to reproduce.

The goal of this paper is two-fold. The first goal is to reveal the connections and differences between the slope/aspect based method of Nuth and Kääb and the terrain gradient based DEM co-registration algorithm of Rosenholm and Torlegard, and the second goal is to present a non-parametric approach to remove the complex systematic errors in DEM co-registration results. The rest of this paper is organized as follows. Sections 2 and 3 introduce and analyze the main co-registration and residual correction methods. Section 4 provides the experimental results, and Sect. 5 concludes the paper.

2. DEM co-registration

The performance of different types of DEM co-registration methods has been intensively investigated by Paul et al. (2015) and Vacaflor et al. (2022). Their tests showed that the method of Nuth and Kääb achieved similar or better accuracy compared to the grid search method (Paul et al., 2015), the LS3D method (Paul et al., 2015), and the subwatershed-based method (Vacaflor et al., 2022), and it was recommended for practical applications due to the less computational effort (Paul et al., 2015). This paper focuses on the analytical (i.e., the terrain information based) methods only. In this section, we will demonstrate that the method of Nuth and Kääb (2011) and the method of Rosenholm and Torlegard (1988) are theoretically compatible. As the original algorithms in the works of Nuth and Kääb (2011) and Rosenholm and Torlegard (1988) were presented in distinct forms, we will present detailed derivations of the equations used in their algorithms and variants.

2.1. The method of Nuth and Kääb

2.1.1. Standard version

The equations of the method of Nuth and Kääb are derived from the geometric relationship (cf. Fig. 1) of the elevation differences induced by the DEM shift with respect to the terrain slope (θ) and aspect (ψ) values. Firstly, we consider the special case where $b=\psi$ (where b is the aspect of the shift vector), i.e., the translation is exactly along the terrain aspect direction. As shown in Fig. 1b, the induced elevation difference is given by:

$$\begin{aligned} dH &= dH_{XY} + dH_Z \\ &= \text{FE}+\text{EG} \\ &= \text{OE}\cdot\tan(\theta)+\text{EG} \\ &= a\cdot\tan(\theta)+c \end{aligned} \tag{1}$$

where a and c are the horizontal and vertical distances of the shift vector, respectively.

In a more general scenario, $b \neq \psi$. As shown in Fig. 1a, the horizontal shift vector **OE'** is decomposed into **OE** and **EE'**. Since **EE'** is perpendicular to the vertical plane OEF defined by the gradient vector and the terrain aspect direction, this does not cause any elevation change. The vertical difference induced by **OE'** is therefore equal to that of **OE**, and it exists:

$$\begin{aligned} dH &= \mathrm{FE} + \mathrm{EG} \\ &= \mathrm{OE} \cdot \tan(\theta) + \mathrm{EG} \\ &= \mathrm{OE'} \cdot \cos(b-\psi)\tan(\theta) + \mathrm{E'G'} \\ &= a \cdot \cos(b-\psi)\tan(\theta) + c \end{aligned} \tag{2}$$

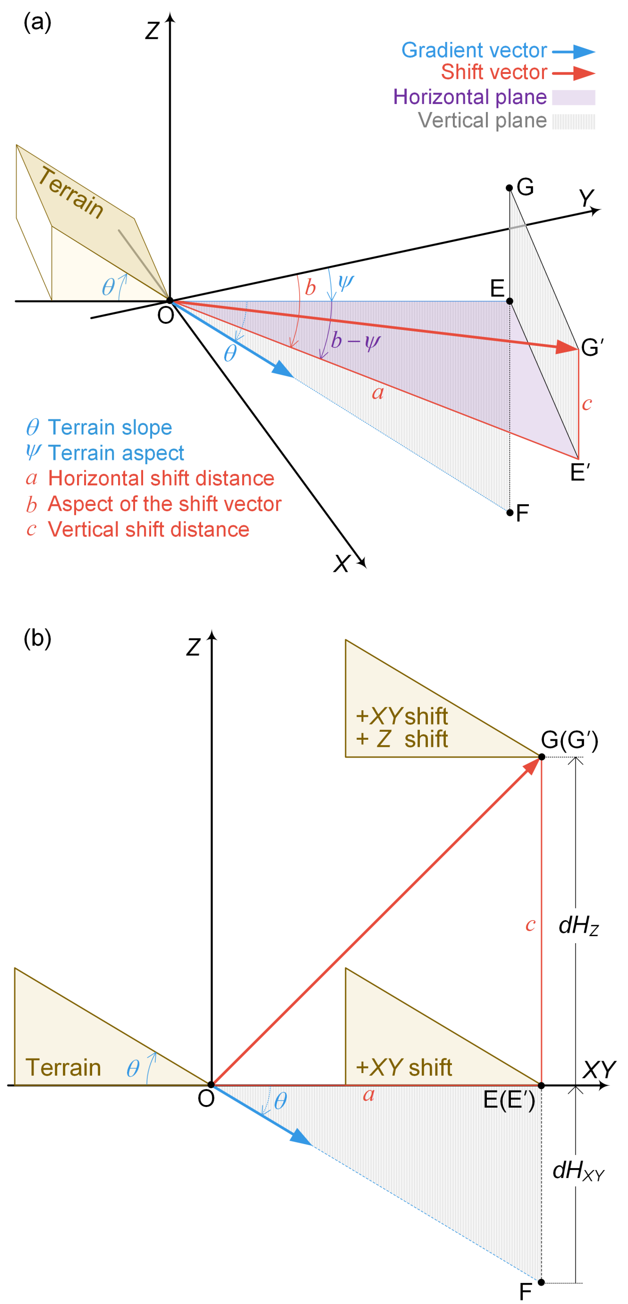

Figure 1. Elevation differences induced by DEM shift. **(a)** 3-D view when $b \neq \psi$. **(b)** 2-D view when $b = \psi$.

The above is Equation (2) in Nuth and Kääb (2011). In this paper, we refer to this as the standard version of the method of Nuth and Kääb. The cylindrical coordinates (a, b, c) of the shift vector can be estimated from a nonlinear regression of Eq. (2), and the corresponding Cartesian coordinates are then given by:

$$
\begin{aligned}
\Delta X &= a \cdot \sin(b) \\
\Delta Y &= a \cdot \cos(b) \\
\Delta Z &= c
\end{aligned}
\tag{3}
$$

As shown in Fig. 2, an iterative process is generally required for accurate co-registration of two DEMs (Nuth and Kääb, 2011), where the coordinates of the ~~slave~~secondary DEM are updated in every iteration by the following equation:

$$
\begin{bmatrix} X \\ Y \\ Z \end{bmatrix}_i = \begin{bmatrix} X \\ Y \\ Z \end{bmatrix}_{i-1} + \begin{bmatrix} \Delta X \\ \Delta Y \\ \Delta Z \end{bmatrix}
\tag{4}
$$

where the subscript i represents the i-th iteration. The iterative process terminates when the change in the dispersion characteristics (median absolute deviation from zero) of the elevation differences between iterations is less than a predefined threshold.

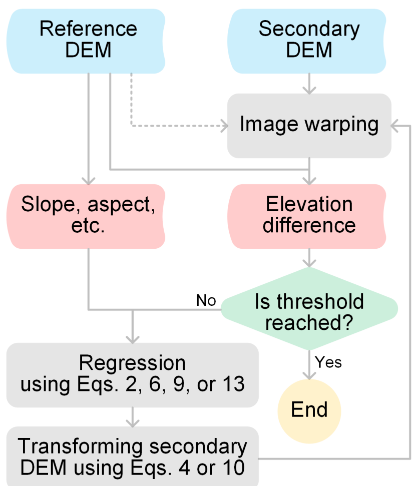

Figure 2. DEM co-registration flowchart.

2.1.2. Simplified version

Nuth and Kääb (2011) did not use Eq. (2) in their experiments, but instead adopted a simplified regression equation by dropping one explanatory variable (θ). Firstly, both sides of Eq. (2) are divided by $\tan(\theta)$:

$$
\frac{dH}{\tan(\theta)} = a \cdot \cos(b - \psi) + \frac{c}{\tan(\theta)}
\tag{5}
$$

θ in the right side of the equation is then approximately replaced by the mean terrain slope of the DEM:

$$
\frac{dH}{\tan(\theta)} \approx a \cdot \cos(b - \psi) + c'
\tag{6}
$$

where

$$c' = \frac{c}{\tan\left(\mathrm{mean}\left(\theta\right)\right)} \tag{7}$$

Accordingly, the shift vector in the Cartesian coordinate system is given by:

$$\begin{aligned} \Delta X &= a \cdot \sin\left(b\right) \\ \Delta Y &= a \cdot \cos\left(b\right) \\ \Delta Z &= c' \cdot \tan\left(\mathrm{mean}\left(\theta\right)\right) \end{aligned} \tag{8}$$

The advantage of the simplified version of the method of Nuth and Kääb (Eq. (6)) is that only one explanatory variable (ψ) exists in the regression model, and the shift vector can therefore be calculated by a curve-fitting technique or estimated from a scatter plot, which is easy to adopt for users with a limited knowledge of statistics.

2.1.3. Linear version

The standard version of the method of Nuth and Kääb can be converted to a linear regression equation by combining Eq. (2) with Eq. (3):

$$\begin{aligned} dH &= a \cdot \cos\left(b-\psi\right)\tan\left(\theta\right)+c \\ &= a \cdot \left(\sin\left(b\right)\sin\left(\psi\right)+\cos\left(b\right)\cos\left(\psi\right)\right)\tan\left(\theta\right)+c \\ &= \sin\left(\psi\right)\tan\left(\theta\right)\Delta X+\cos\left(\psi\right)\tan\left(\theta\right)\Delta Y+\Delta Z \end{aligned} \tag{9}$$

This equation uses $\Delta X, \Delta Y$, and ΔZ as the regression coefficients directly, and, accordingly, the conversion of the shift vector from cylindrical coordinates to Cartesian coordinates is no longer required.

2.2. The method of Rosenholm and Torlegard

In the method of Rosenholm and Torlegard, the misalignment between two DEMs is described by a 3-D similarity transformation (Molodenskii, 1962; Badekas, 1969), and the coordinate update equation for the ~~slave~~secondary DEM is:

$$\begin{bmatrix} X_{\mathrm{C}} \\ Y_{\mathrm{C}} \\ Z_{\mathrm{C}} \end{bmatrix}_i = \left(1+\gamma\right)\begin{bmatrix} 1 & -\kappa & \varphi \\ \kappa & 1 & -\omega \\ -\varphi & \omega & 1 \end{bmatrix}\begin{bmatrix} X_{\mathrm{C}} \\ Y_{\mathrm{C}} \\ Z_{\mathrm{C}} \end{bmatrix}_{i-1} + \begin{bmatrix} \Delta X \\ \Delta Y \\ \Delta Z \end{bmatrix} \tag{10}$$

where γ is the scale factor; ω, φ, and κ are the rotation angles (in radians) about the *X*, *Y*, and *Z* axes, respectively; and the subscript C refers to the coordinates being zero-centered. Note that the values of γ, ω, φ, and κ are relatively small in the DEM co-registration process. The coordinate changes in each iteration can be approximated as:

$$\begin{bmatrix} X_{\mathrm{C}} \\ Y_{\mathrm{C}} \\ Z_{\mathrm{C}} \end{bmatrix}_i - \begin{bmatrix} X_{\mathrm{C}} \\ Y_{\mathrm{C}} \\ Z_{\mathrm{C}} \end{bmatrix}_{i-1} \approx \begin{bmatrix} \Delta X+\gamma X_{\mathrm{C}}-\kappa Y_{\mathrm{C}}+\varphi Z_{\mathrm{C}} \\ \Delta Y+\kappa X_{\mathrm{C}}+\gamma Y_{\mathrm{C}}-\omega Z_{\mathrm{C}} \\ \Delta Z-\varphi X_{\mathrm{C}}+\omega Y_{\mathrm{C}}+\gamma Z_{\mathrm{C}} \end{bmatrix} \tag{11}$$

By comparing Eq. (11) with Eq. (4), it can be seen that the coordinate change of every DEM pixel is a constant vector ($\Delta X, \Delta Y, \Delta Z$) in the method of Nuth and Kääb, while it varies with the position (X_C, Y_C, Z_C) in the method of Rosenholm and Torlegard. Accordingly, the following equation is derived by substituting Eq. (11) into Eq. (9):

$$dH = \sin(\psi)\tan(\theta)(\Delta X + \gamma X_C - \kappa Y_C + \varphi Z_C) + \cos(\psi)\tan(\theta)(\Delta Y + \kappa X_C + \gamma Y_C - \omega Z_C) + (\Delta Z - \varphi X_C + \omega Y_C + \gamma Z_C) \quad (12)$$

By rearranging the above equation, the DEM elevation differences caused by translation, scaling, and rotation can be obtained as:

$$dH = v_{\Delta X}\Delta X + v_{\Delta Y}\Delta Y + \Delta Z + v_\gamma \gamma + v_\omega \omega + v_\varphi \varphi + v_\kappa \kappa \quad (13)$$

where

$$\begin{aligned} v_{\Delta X} &= \sin(\psi)\tan(\theta) \\ v_{\Delta Y} &= \cos(\psi)\tan(\theta) \\ v_\gamma &= v_{\Delta X} X_C + v_{\Delta Y} Y_C + Z_C \\ v_\omega &= Y_C - v_{\Delta Y} Z_C \\ v_\varphi &= v_{\Delta X} Z_C - X_C \\ v_\kappa &= v_{\Delta Y} X_C - v_{\Delta X} Y_C \end{aligned} \quad (14)$$

It can be found from the geoscience literature that the slope and aspect angles relate to the terrain gradients, and the following equation (Peckham and Jordan, 2007) exists when the terrain aspect is measured clockwise from north:

$$\begin{aligned} \theta &= \arctan\sqrt{f_X^2 + f_Y^2} \\ \psi &= \pi - \arctan\left(\frac{f_Y}{f_X}\right) + \frac{\pi}{2}\left(\frac{f_X}{|f_X|}\right) \end{aligned} \quad (15)$$

where f_X and f_Y are the gradients of the terrain in the X and Y directions, respectively. From the above equation, we obtain:

$$\begin{aligned} f_X &= -\sin(\psi)\tan(\theta) \\ f_Y &= -\cos(\psi)\tan(\theta) \end{aligned} \quad (16)$$

Finally, by substituting Eq. (16) into Eq. (14), Eq. (13) is as follows:

$$dH = -f_X \Delta X - f_Y \Delta Y + \Delta Z + v_\gamma \gamma + v_\omega \omega + v_\varphi \varphi + v_\kappa \kappa \quad (17)$$

The above equation is Equation (6) in Rosenholm and Torlegard (1988).

2.3. Discussion

The characteristics of the method of Nuth and Kääb and the method of Rosenholm and Torlegard are summarized in Table 1, and the connections and differences between them are discussed in the following.

Table 1. Summary of the main DEM co-registration methods.

Method	ID*	Regression equation	Explanatory variables	Regression coefficients

Nuth and Kääb standard version	N23	(2)	ψ, θ	a, b, c
Nuth and Kääb simplified version	N13	(6)	ψ	a, b, c'
Nuth and Kääb linear version	L23	(9)	ψ, θ	$\Delta X, \Delta Y, \Delta Z$
Rosenholm and Torlegard	L57	(17)	f_X, f_Y, X_C, Y_C, Z_C	$\Delta X, \Delta Y, \Delta Z, \gamma, \omega, \varphi, \kappa$

* A three-digit alphanumeric code to identify each method, where N and L represent nonlinear and linear regression, respectively; 1, 2, or 5 is the number of explanatory variables; and 3 or 7 is the number of regression coefficients.

1) The form of the regression

The method of Nuth and Kääb can be expressed as either a nonlinear (N23 or N13) or linear (L23) equation, while the method of Rosenholm and Torlegard only employs a linear regression model (L57). The disadvantages of nonlinear regression over linear regression are that it works iteratively and it requires starting values for the coefficients to be determined. For the N23 and N13 methods, the unknown coefficients can be initialized by:

$$\begin{aligned} a_0 &= 0 \\ b_0 &= 0 \\ c_0 &= \text{mean}\left(dH\right) \end{aligned} \tag{18}$$

and

$$\begin{aligned} a_0 &= 0 \\ b_0 &= 0 \\ c_0' &= \frac{\text{mean}\left(dH\right)}{\tan\left(\text{mean}\left(\theta\right)\right)} \end{aligned} \tag{19}$$

, respectively.

2) The explanatory variables in the regression

The method of Nuth and Kääb was inspired by the similarity between an elevation difference map and a hillshade, which is predicted based on the terrain slope and aspect. The method of Rosenholm and Torlegard, on the other hand, employs the terrain gradients (i.e., the partial first derivatives) in the X and Y directions as the explanatory variables. From Eqs. (15) and (16), it can be seen that the two groups of terrain variables are actually equivalent.

3) Regression coefficients

In the method of Rosenholm and Torlegard, the misalignment between two DEMs is modeled by a 3-D similarity transformation, including three translation, one scale, and three rotation factors. The method of Nuth and Kääb considers the spatial shift only, and the regression coefficients can be either cylindrical coordinates (a, b, c) or Cartesian coordinates ($\Delta X, \Delta Y, \Delta Z$) of the shift vector.

Based on the above analysis, it can be concluded that the number of regression coefficients is the only significant difference between the method of Nuth and Kääb and the method of Rosenholm and Torlegard. In other words, the method of Rosenholm and Torlegard can be viewed as an extension of the method of Nuth and Kääb by additionally modeling the scale and rotation errors.

3. Residual correction

A residual correction procedure is highly recommended after DEM co-registration (Berthier et al., 2007; Leprince et al., 2007) because some systematic errors related to the terrain height and satellite acquisition geometry (along-track and cross-track) often remain. As elevation-dependent biases were not observed in our experiments, the following section introduces the residual correction algorithms for the along-track and cross-track directions only.

3.1. Parametric regression

High-order polynomial (6th to 8th order) regression is the most commonly used way to fit DEM co-registration residuals (Nuth and Kääb, 2011; Gardelle et al., 2013; Berthier et al., 2016; Brun et al., 2017), and is usually performed in a stepwise manner:

$$\begin{aligned} dH_{X_t} &= \sum_{i=0}^{m} P_i X_t^{\,i} \\ dH_{Y_t} &= \sum_{j=0}^{m} P_j Y_t^{\,j} \end{aligned} \tag{20}$$

with

$$\begin{aligned} X_t &= X\cos(\theta_t) - Y\sin(\theta_t) \\ Y_t &= X\sin(\theta_t) + Y\cos(\theta_t) \end{aligned} \tag{21}$$

where X_t and Y_t are the cross-track and along-track coordinates, respectively; θ_t is the angle between the along-track direction and the north; m is the degree of the polynomial; and P_i and P_j are the coefficients to be estimated.

Many previous studies have reported that the residual signals in the along-track direction often appear at one to three frequencies, and are most likely induced by satellite attitude jitter, which is mainly caused by high-frequency mechanical vibration (Leprince et al., 2007; Nuth and Kääb, 2011). Girod et al. (2017) pointed out that these periodic residuals can be modeled by a sum of the sinusoidal functions:

$$\begin{aligned} dH_{X_t} &= \sum_{i=0}^{m} P_i X_t^{\,i} \\ dH_{Y_t} &= \sum_{k=1}^{n} A_k \sin\left(2\pi f_k Y_t + \varphi_k\right) \end{aligned} \tag{22}$$

where n is the number of sinusoidal functions; and A_k, f_k, and φ_k are the amplitude, frequency, and phase of the k-th sinusoidal component, respectively.

3.2. Non-parametric regression

We propose an alternative residual correction method using a generalized additive model (GAM):

$$dH = s\left(X_t\right) + s\left(Y_t\right) \tag{23}$$

where $s(*)$ represents a smooth function. As an extension of the linear model by including additive smooth functions for the explanatory variables, the GAM has the potential to capture complex nonlinear patterns that a parametric model (e.g., high-order polynomials and sinusoidal functions) would miss.

The GAM software packages are widely available in various programming languages, such as R, Python, Matlab, and SAS. Typical smooth functions include local polynomials, splines, Markov Random Fields, and Gaussian process smooths. In our experiments, the GAM regression of Eq. (23) was performed in R software using the 'mgcv' package (Wood, 2022). A thin-plate spline was chosen as the smoothing basis (i.e., the smooth function s), and the degree of smoothing was automatically determined by the generalized cross validation (GCV) criterion. For more on the theoretical foundations and technical details of the GAM method and the 'mgcv' package, we refer the reader to Hastie and Tibshirani (1990) and Wood (2017).

4. Experiments

4.1. Ice Sheet case study

~~4.1.~~4.1.1. Data processing

~~All the algorithms introduced in the last two sections were compared using 23 Advanced Spaceborne Thermal Emission and Reflection Radiometer (ASTER) DEM pairs from the western edge of the Greenland Ice Sheet (Fig. 3). Details of two of the DEM pairs are provided in Table 2.~~ The comparative experiments of DEM co-registration and residual correction were carried out on 23 Advanced Spaceborne Thermal Emission and Reflection Radiometer (ASTER) DEM pairs from the western edge of the Greenland Ice Sheet (GrIS) (Fig. 3). Details of all ASTER DEM pairs are provided in the Supplement (Table S1), where two DEM pairs were used for visualization and analysis (Table 2). The raw stereoscopic DEMs were automatically produced by the US Geological Survey Land Processes Distributed Active Archive Center (LPDAAC) using SilcAst software (NASA et al., 2001).

~~The experimental workflow is shown in Fig. 4. Firstly, t~~The normalized difference bareness index (NDBI) was calculated from Landsat 8 images to extract stable regions (Nguyen et al., 2021):

$$\mathrm{NDBI} = \frac{\mathrm{SWIR1} - \mathrm{G}}{\mathrm{SWIR1} + \mathrm{G}} \tag{24}$$

where SWIR1 and G represent the first shortwave infrared band (1.560–1.660 μm) and the green band (0.525–0.600 μm) of the Landsat 8 Operational Land Imager (OLI) data, respectively. All the terrain-related information (slope, aspect, etc.), which served as explanatory variables of the regression, was then derived from the ~~master~~reference DEMs. In the co-registration and residual correction procedures, only DEM pixels over stable terrain were used for the regression, and a three-sigma rule (i.e., more than three times the standard deviation) was employed on the elevation differences between two DEMs to remove erroneous data caused by misclassification of unstable terrain areas. A subset of the data (of no more than 50,000 pixels, to reduce the computational cost) was randomly selected as the training set, and the remaining pixels were used for the accuracy evaluation by comparing the median absolute difference (MedAD) (Mcmillan et al., 2019; Trevisani and Rocca, 2015):

$$\text{MedAD} = \text{median}\left(\left|H_{\text{Reference}} - H_{\text{Secondary}}\right|\right) \quad (25)$$

where $H_{\text{Reference}}$ and $H_{\text{Secondary}}$ represent the ~~master~~reference and ~~slave~~secondary DEM elevation, respectively.

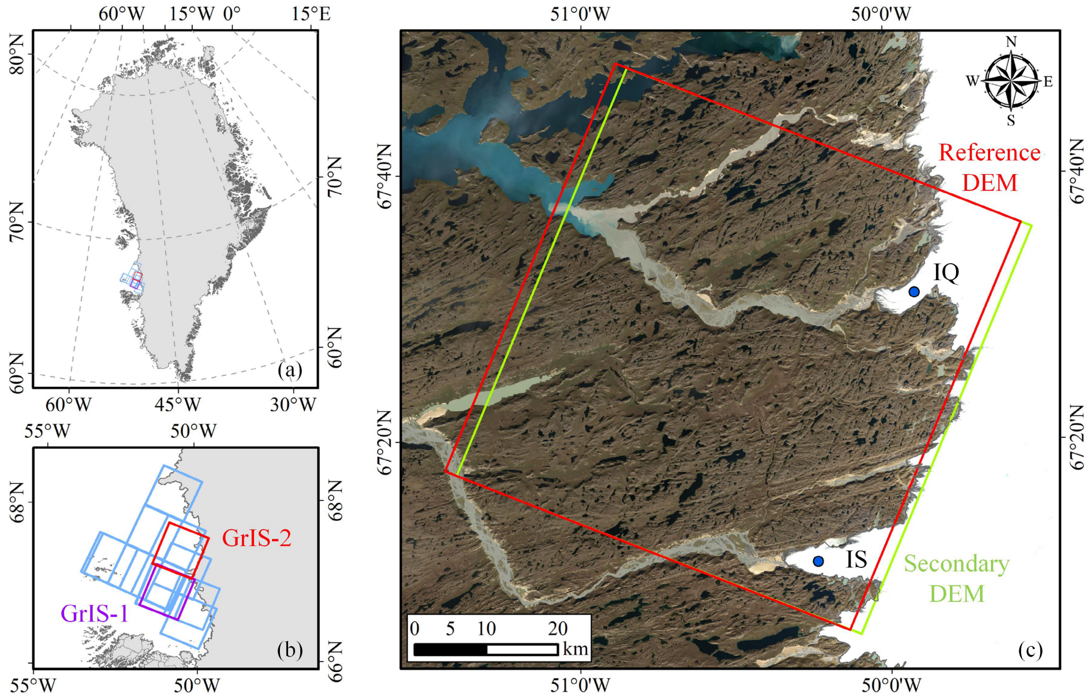

Figure 3. The study area located on the western edge of ~~the Greenland Ice Sheet~~GrIS. **(a)** and **(b)** The footprints (blue) of the 23 ASTER DEM pairs, where pairs ~~A~~GrIS-1 and ~~B~~GrIS-2 listed in **Table 2** are highlighted in purple and red, respectively. **(c)** The coverage of the two DEM images in pair ~~B~~GrIS-2 (red: ~~master~~reference DEM; green: ~~slave~~secondary DEM). IQ and IS are the Inugpait Quat Glacier and Isunguata Sermia Glacier, respectively. The background image was acquired by Landsat 8 in 2016.

Table 2. Characteristics of the two DEM pairs in GrIS.

Pair ID	Roles	Date	Res. (m)	Scene ID
~~A~~GrIS-1	~~Master~~Reference DEM	5 Aug 2014	30	AST14DEM.003:2133338256
	~~Slave~~Secondary DEM	7 Aug 2003	30	AST14DEM.003:2015893657
~~B~~GrIS-2	~~Master~~Reference DEM	25 Jul 2016	30	AST14DEM.003:2237110490
	~~Slave~~Secondary DEM	17 Jun 2002	30	AST14DEM.003:2007321075

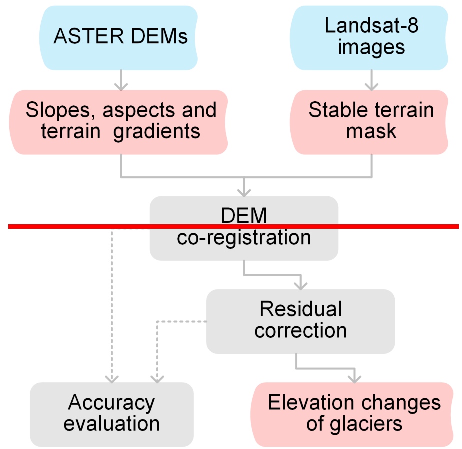

~~**Figure 4.** The workflow of the DEM co-registration and residual correction experiments.~~

~~4.2. Results and analysis~~

~~4.2.1.~~4.1.2. DEM co-registration

Table 3 shows that all four co-registration methods effectively reduce the DEM biases, and the following findings were made by comparing the error statistics of the different algorithms.

1) The standard and linear versions of the method of Nuth and Kääb yield exactly the same outcomes. The only difference between the two algorithms (L23 and N23) is whether the regression equation is linear or not, which does not affect the co-registration results.

2) The simplified version of the method of Nuth and Kääb produces similar results to the standard version. It should be noted that this conclusion may not hold true for other datasets, because it cannot be proven theoretically that approximating terrain slopes by their mean value would always lead to a reliable performance.

3) The method of Rosenholm and Torlegard performs better than the three versions of the method of Nuth and Kääb. The co-registration errors of L57 are smaller than those of L23 by an average of 4.6% and a maximum of 15.3%, which indicates that there are some scale- and rotation- induced biases in the experimental DEM data.

Table 3. Co-registration results obtained with the 23 DEM pairs of GrIS.

Method	ID	Average MedAD (m)
Before co-registration	—	12.043
Nuth and Kääb standard version	N23	7.170
Nuth and Kääb simplified version	N13	7.163
Nuth and Kääb linear version	L23	7.170
Rosenholm and Torlegard	L57	6.839

~~Figure 5~~ Figure 4 shows the elevation differences of DEM pair ~~A~~GrIS-1 before co-registration. All the pixels classified as water and potential outliers due to clouds were masked out for a better visualization, leaving the regions of bare land and glacier (bounded by the black lines). It can be seen from the figure that most pixels are negative values, indicating that the majority of the elevation differences are caused by vertical translation. Minor errors related to the terrain (induced by horizontal translation) and along-track coordinates (caused by jitter) can also be clearly observed.

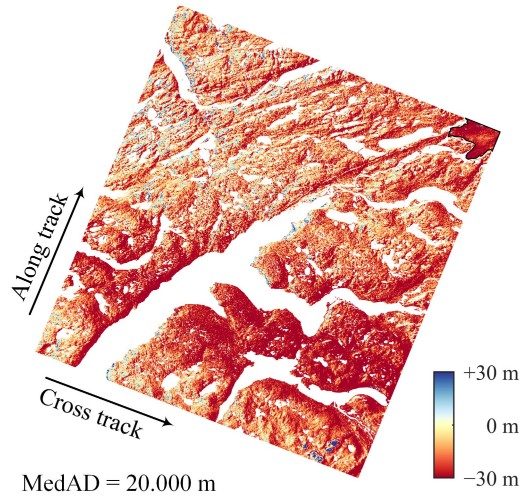

Figure ~~5~~4. The elevation differences before DEM co-registration (pair ~~A~~GrIS-1). The black lines mark the glacier boundaries.

The elevation difference maps (Fig. ~~6~~5) demonstrate that the residuals of all three versions of the Nuth and Kääb co-registration algorithms are consistent in terms of both magnitude and distribution. The Rosenholm and Torlegard algorithm shows better co-registration results, with an accuracy improvement of 11.8% compared to the linear version of Nuth and Kääb. A visual inspection of Fig. ~~6~~5 c and d reveals that the elevation differences of the method of Nuth and Kääb exhibit a positive trend in the northwest corner (the blue circle in Fig. ~~6~~5c) and a negative trend in the southeast corner (the red circle in Fig. ~~6~~5c), which are possibly caused by unconsidered attitude biases. In addition, some clustered outliers, which may consist of misclassified water and cloud pixels, can be clearly observed in the elevation difference maps (Fig. ~~6~~5a). However, these outliers have little influence on the co-registration results because robust statistical methods (robust regression algorithms and a robust scale estimation method, i.e., MedAD) were used in the experiments.

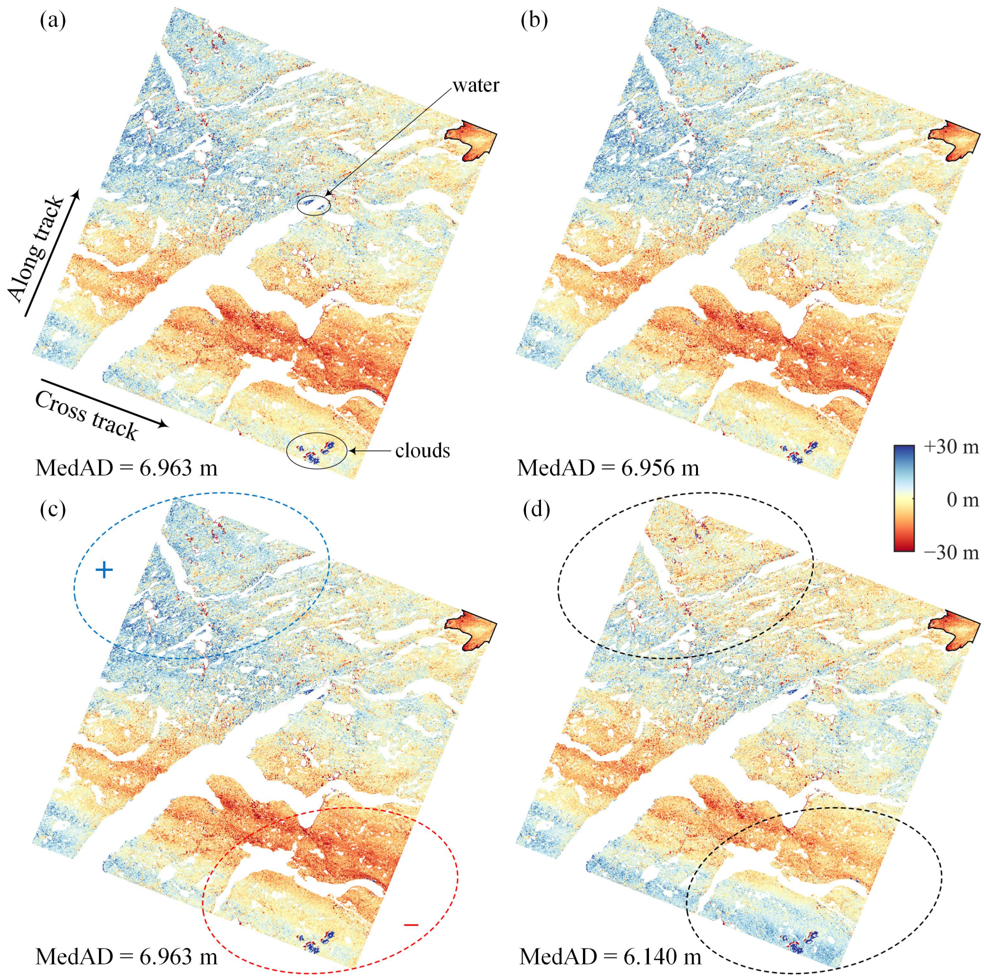

Figure ~~6~~5. Co-registration results of the different methods for DEM pair ~~A~~GrIS-1: the standard **(a)**, simplified **(b)**, and linear **(c)** versions of the method of Nuth and Kääb, and the method of Rosenholm and Torlegard **(d)**.

~~4.2.2.~~4.1.3. Residual correction

The residual correction results for DEM pair ~~A~~GrIS-1 are shown in Fig. ~~7~~6. In the experiments, the polynomial fitting method used an 8th-order polynomial sequentially in the cross-track and along-track directions, and the combination of polynomial and the sum of sines method was implemented by first adopting an 8th-order polynomial in the cross-track direction and then applying a sum of three sines in the along-track direction. A visual comparison reveals that the high-order polynomial removes the low-frequency residuals only, whereas both the sum of sines and the GAM spline can capture the high-frequency signals. The MedAD values show that the GAM spline fitting method yields a higher accuracy than the two parametric regression methods.

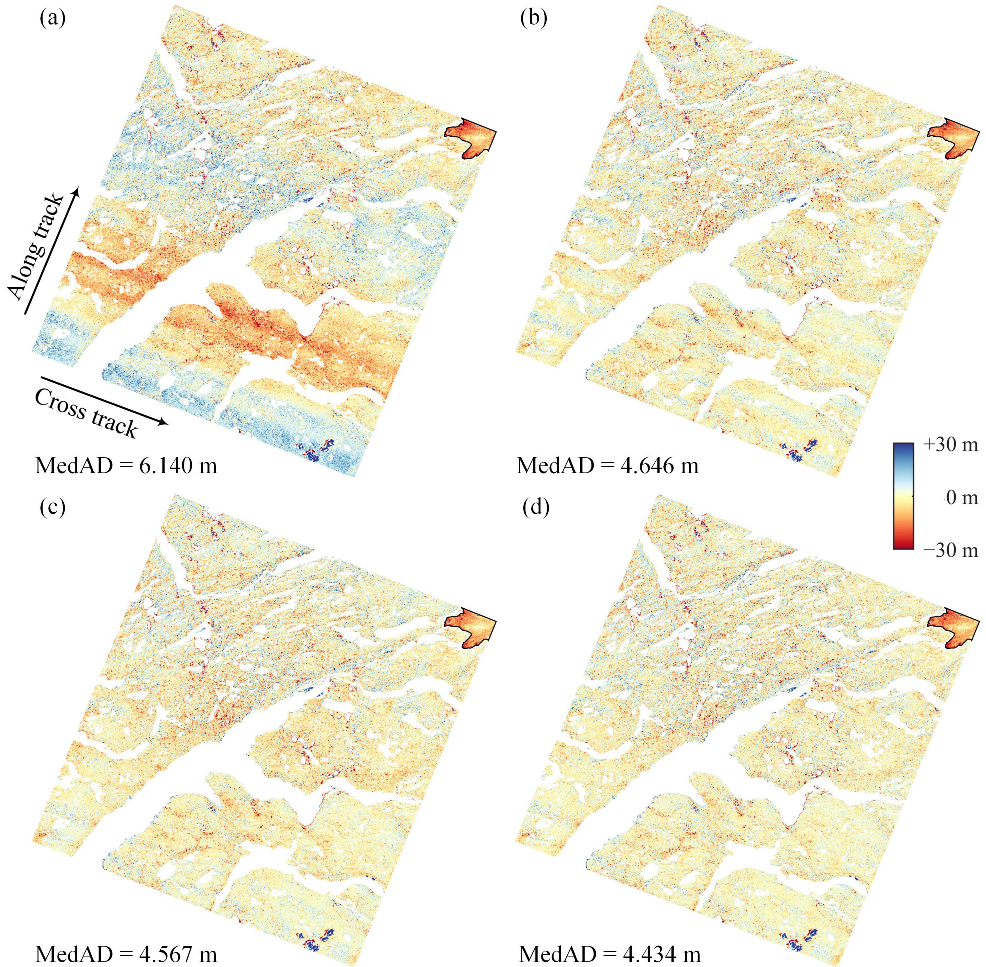

Figure ~~7~~6. Residual correction of DEM pair ~~A~~GrIS-1. **(a)** The DEM co-registration results obtained using the method of Rosenholm and Torlegard. The residual correction results obtained using polynomial fitting **(b)**, the combination of polynomial and the sum of sines method **(c)**, and GAM spline fitting **(d)**.

The magnitude of the high-frequency signals in DEM pair ~~B~~GrIS-2 is much greater than that in DEM pair ~~A~~GrIS-1 in Fig. ~~8~~7b. The polynomial fitting method again eliminates only the low-frequency residuals. ~~Figure 8~~Figure 7 c and d show that weak striped patterns exist in the residual results of both the sum of sines and the GAM spline fitting methods, indicating that the high-frequency errors are not completely removed. The MedAD values show that the combination of polynomial and the sum of sines method is 5.1% less accurate than the GAM-based method, which can be observed by the significant negative biases indicated by the arrows in Fig. ~~8~~7c. ~~Figure 9~~Figure 8 further shows the fitting results in the along-track direction. The 8th-order polynomial only matches the long-term trend, and a follow-up experiment revealed that increasing the order of the polynomial still does not help to capture high-frequency signals. As marked by the red and purple arrows in Fig. ~~9~~8 (corresponding to the regions indicated in Fig. ~~8~~7), the maximum difference between the sum of sines and the GAM spline fitting results is about 5 m. Because the sinusoidal function is a parametric model whose parameters (amplitude, phase, and frequency) are global constants, there is no difference in shape between the different cycles. In contrast, the GAM spline yields a non-strictly periodic curve by fitting the local relationship between the elevation differences (the response variable) and the along-track coordinates (the predictor variable) over parts of their range. A visual inspection shows that the GAM spline fitting results fit more closely with the local trends in the co-registration residuals, which indicates that the GAM spline fitting method might be a better alternative to the traditional parametric models for residual correction of DEM co-registration results, benefiting from its data-driven nature.

Finally, Table 4 summarizes the residual correction results for the 23 ASTER DEM pairs. The GAM spline fitting method outperforms the polynomial method and the combination of polynomial and the sum of sines method by reducing 4.4% and 2.1% more residuals, respectively. We manually check~~ed~~ the residual correction results for all the DEM pairs. A visual inspection shows that the remaining errors for a majority of the data (e.g., pair ~~A~~GrIS-1 in Fig. ~~7~~6) are almost randomly distributed in the scene. Only a few DEM pairs suffer from minor systematic errors caused by incompletely corrected jitter (e.g., pair ~~B~~GrIS-2 in Fig. ~~8~~7), where slight biases would be propagated into the glacier thickness change estimates.

Table 4. Residual correction results with the 23 DEM pairs of GrIS.

Method	Average MedAD (m)
Polynomial fitting	5.825
Polynomial and the sum of Sines	5.686
GAM spline fitting	5.566

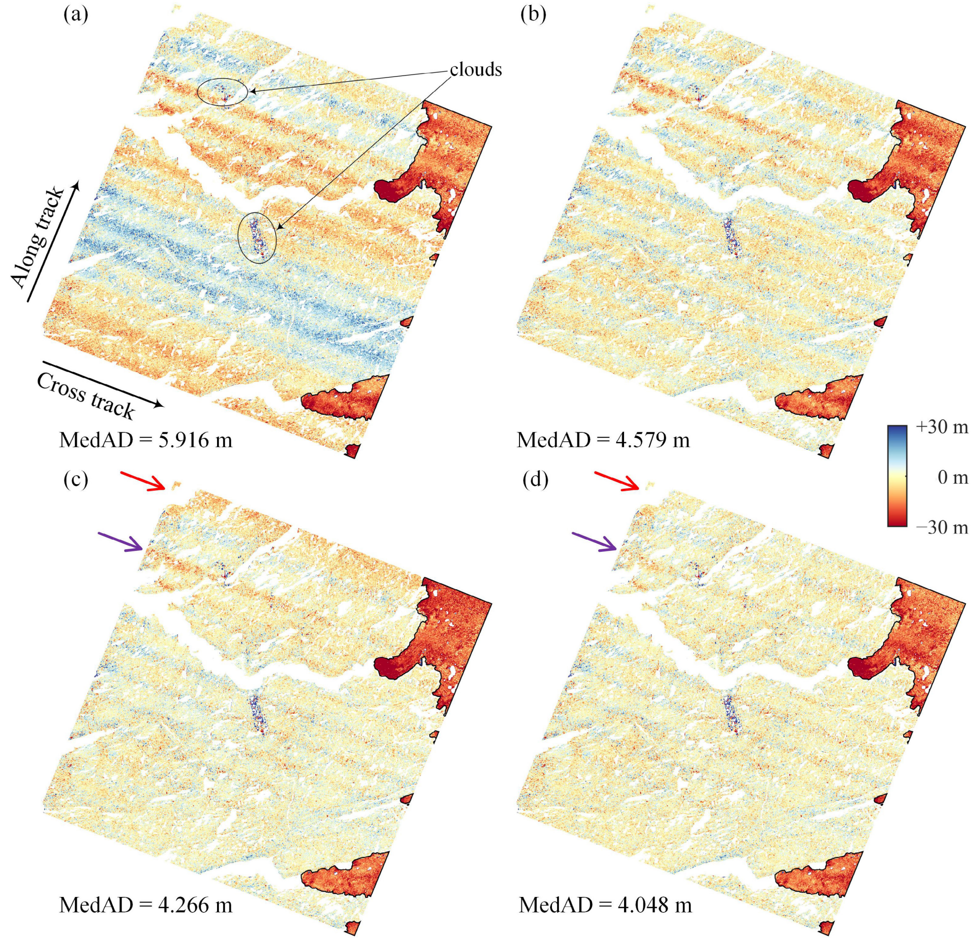

Figure ~~8~~7. Residual correction of DEM pair ~~B~~GrIS-2. **(a)** The DEM co-registration results obtained using the method of Rosenholm and Torlegard. The residual correction results obtained using polynomial fitting **(b)**, the combination of polynomial and the sum of sines method **(c)**, and GAM spline fitting **(d)**.

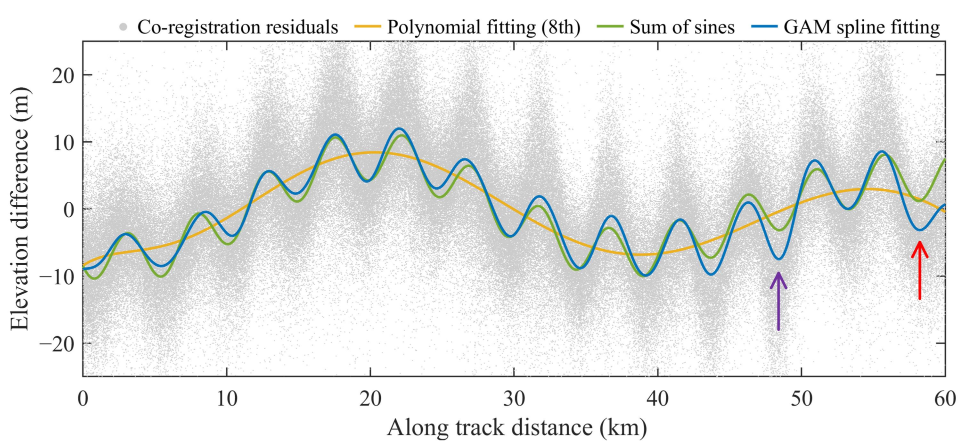

Figure ~~9~~8. Co-registration residuals of DEM pair ~~B~~GrIS-2 and the along-track fitting results.

4.2. Mountain glacier case study

4.2.1. Data processing

The mountain glacier experiments were performed on 22 DEM pairs from the Pamir region of High Mountain Asia (HMA) (Fig. 9), including ASTER DEMs, ZiYuan-3 (ZY-3) DEMs generated from ZiYuan-3 tri-stereo optical scenes (Tang et al., 2018; Liu et al., 2020), and global DEMs Shuttle Radar Topography Mission (SRTM) DEMs (Farr et al., 2007) and Copernicus DEMs GLO30 (Airbus, 2020) obtained using the Interferometric Synthetic Aperture Radar (InSAR) technique. Stable regions were extracted from three land cover classes (bare land, artificial surfaces, and cultivated land) in the GlobeLand30 land cover product (Jun et al., 2014; Li et al., 2021).

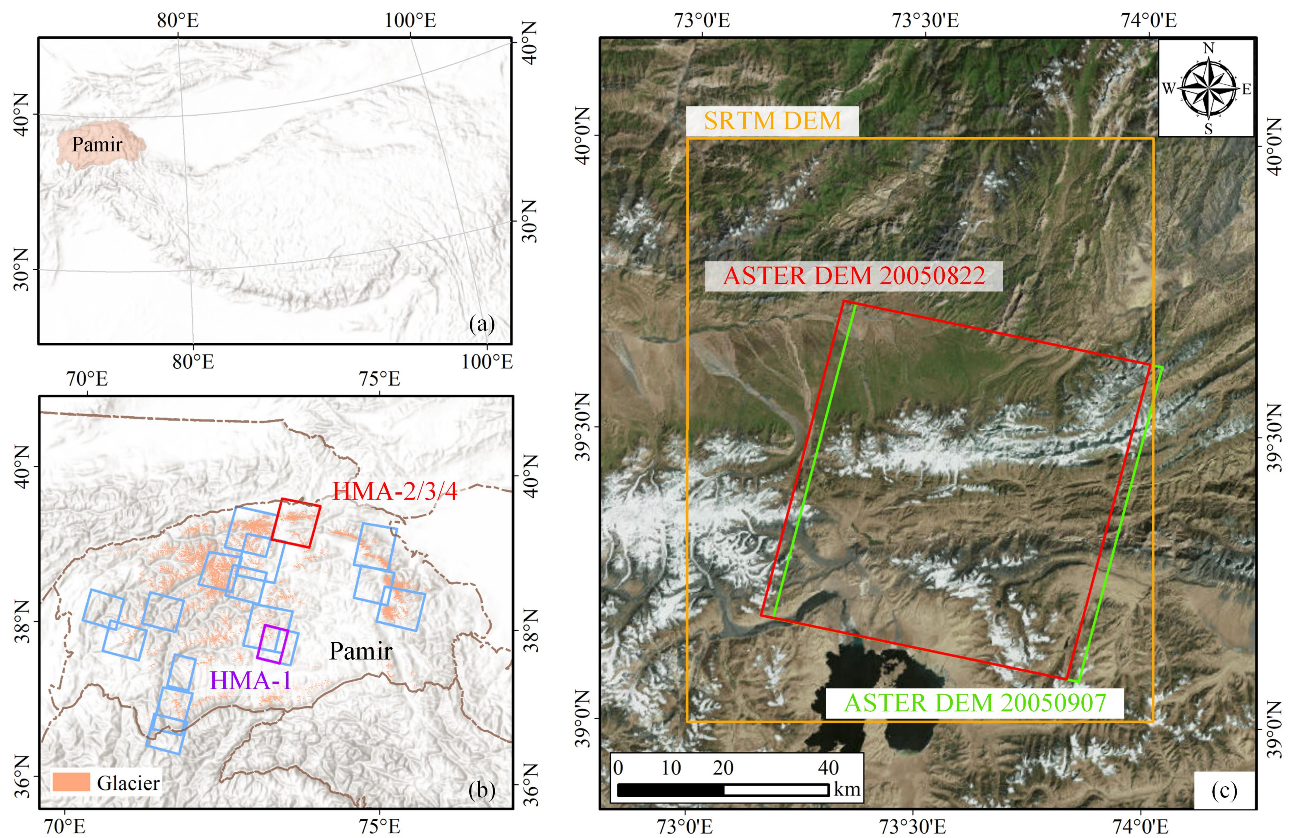

Figure 9. The study area located on HMA. (a) and (b) The footprints (blue) of the 22 DEM pairs, where pairs HMA-1 and HMA-2/3/4 listed in **Table 5** are highlighted in purple and red, respectively. (c) The coverage of the three DEM images in HMA-2/3/4 (orange: SRTM DEM; red: ASTER DEM 20050822; green: ASTER DEM 20050907).

Table 5. Characteristics of the 4 DEM pairs in HMA.

Pair ID	Data	Roles	Date	Res. (m)	Scene ID
HMA-1	Copernicus DEM	Reference DEM	2011–2015	30	N37E073, N38E073
	ZY-3 DEM	Secondary DEM	8 Oct 2017	30	—
HMA-2	SRTM DEM	Reference DEM	11–22 Feb 2000	30	N39E073
	ASTER DEM	Secondary DEM	22 Aug 2005	30	AST14DEM.003:2030590191
HMA-3	ASTER DEM	Reference DEM	22 Aug 2005	30	AST14DEM.003:2030590191
	ASTER DEM	Secondary DEM	7 Sept 2005	30	AST14DEM.003:2030819798
HMA-4	SRTM DEM	Reference DEM	11–22 Feb 2000	30	N39E073
	ASTER DEM	Secondary DEM	7 Sept 2005	30	AST14DEM.003:2030819798

4.2.2. DEM co-registration

Like the Ice Sheet case, the simplified and standard versions of the method of Nuth and Kääb yield similar results for the three test datasets of ZY-3 DEMs, SRTM DEMs, and Copernicus DEMs in the HMA region (Table 6). The method of Rosenholm and Torlegard shows better co-registration performance than the three versions of the method of Nuth and Kääb, with an average accuracy improvement of 13.7% over the linear version.

Table 6. Co-registration results obtained with the 22 DEM pairs of HMA.

Method	ID	Average MedAD (m)
Before co-registration	—	15.483
Nuth and Kääb standard version	N23	7.220
Nuth and Kääb simplified version	N13	7.212
Nuth and Kääb linear version	L23	7.220
Rosenholm and Torlegard	L57	6.230

Figure 10 depicts an example of the ZY-3 DEM with large attitude errors. From Fig. 10 a to c, it can be seen that the co-registration results of the Nuth and Kääb method exhibit significant residuals in the southwest-northeast direction, leading to a false estimate of rapid glacier mass loss in the northern region. In contrast, the Rosenholm and Torlegard algorithm can effectively eliminate attitude-induced bias and reduce co-registration errors by 83.3% compared to the Nuth and Kääb linear version. A visual comparison between Fig. 10d and Fig. 5d reveals that the co-registration residuals of the ZY-3 DEM are much smaller than those of the ASTER DEM. This may be due to the fact that the ZY-3 raw image has a resolution of 2.5–3.5 m (Zhang et al., 2018) and retains a high signal-to-noise ratio after downsampling to 30 m.

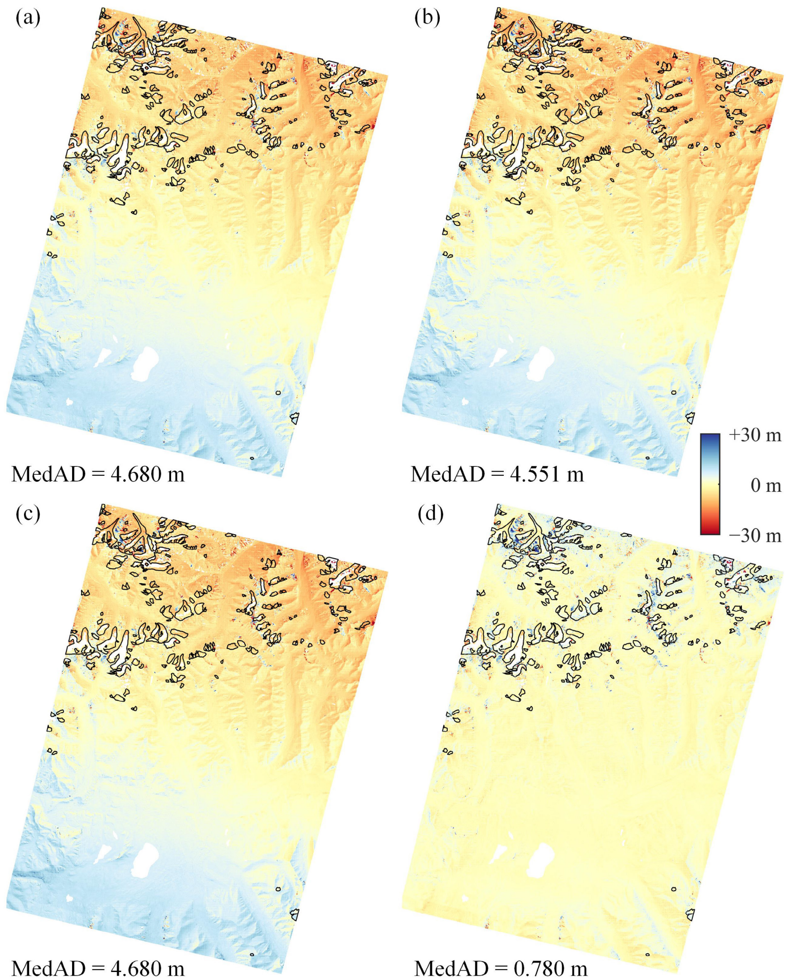

Figure 10. Co-registration results of the different methods for DEM pair HMA-1: the standard (a), simplified (b), and linear (c) versions of the method of Nuth and Kääb, and the method of Rosenholm and Torlegard (d).

Figure 11 illustrates the influence of the DEM co-registration method on glacier surface elevation changes estimation. Subplots b, e, and g show the co-registration results and glacier elevation change statistical values for an ASTER DEM pair acquired half a month apart (HMA-3). Since the two DEMs were obtained at a very short time interval, it can be assumed that there is no elevation change. The result of the Nuth and Kääb linear version contains obvious rotation-induced errors (Fig. 11b), the large proportion of missing data throughout the center of the image are caused by cloud cover, and the glacier-covered area in the southeast region only covers a small number of invalid pixels. We calculated the glacier elevation change values within the red circle and found a significant negative deviation (−6.396 m). No distinct abnormal trends were found in the results of the Rosenholm and Torlegard method, and the mean value of glacier elevation changes is very close to zero. Furthermore, we co-registered these two ASTER DEMs with the SRTM DEM, i.e., the DEM pairs HMA-2 and HMA-4, and their co-registration results are shown in Figs. 11 a/d and c/f, respectively. Theoretically, the glacier elevation changes of

2000–2005 derived from HMA-2 and HMA-4 should be consistent. Figure 11h indicates that the discrepancy in the estimation results of the method of Rosenholm and Torlegard is smaller than that of Nuth and Kääb, with the mean value improving from −5.927 m to −1.669 m.

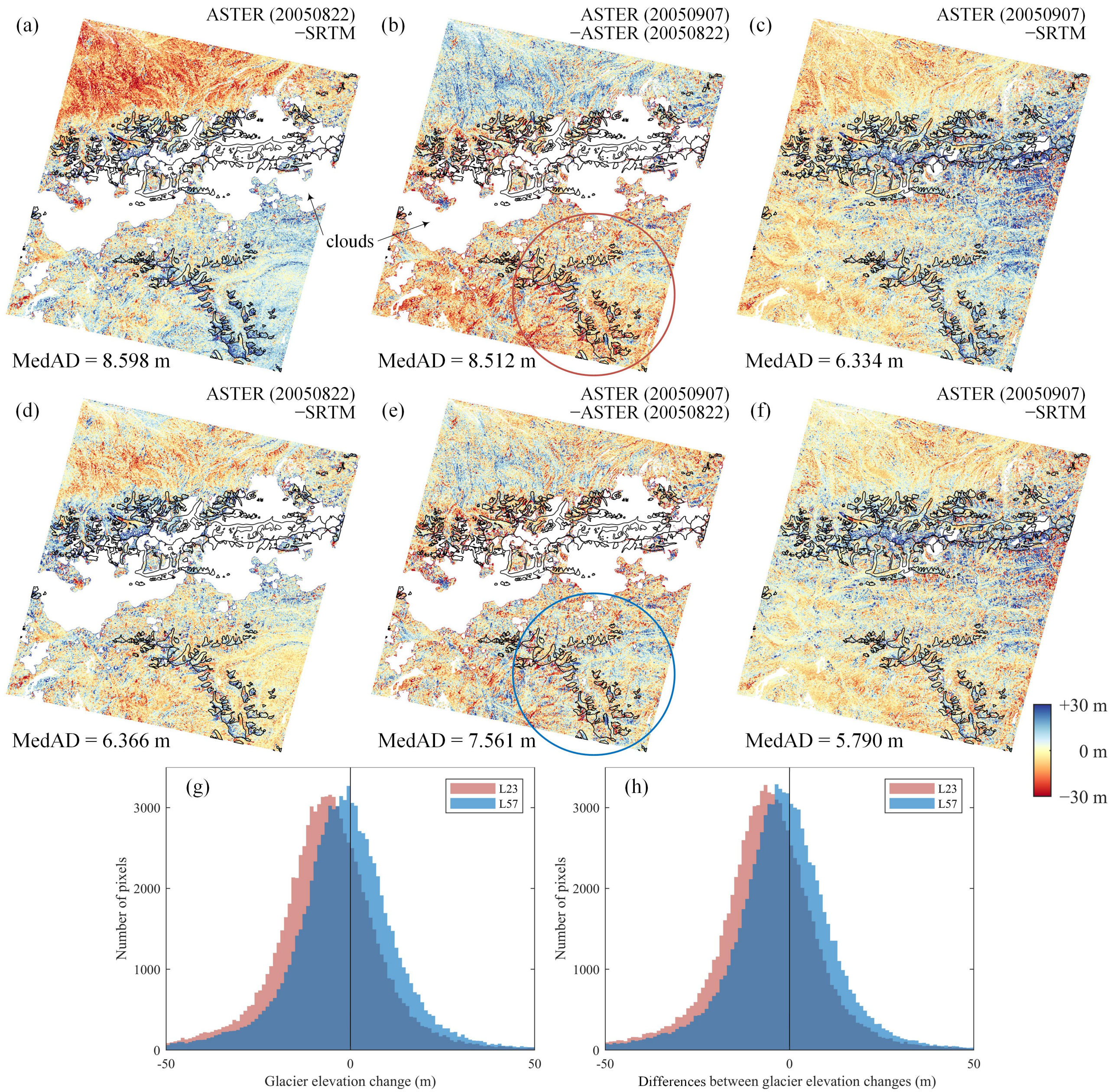

Figure 11. Co-registration results of DEM pairs HMA-2/3/4 based on linear versions of the method of Nuth and Kääb (top) and the method of Rosenholm and Torlegard (middle). From left to right: HMA-2, HMA-3, and HMA-4, respectively. (g) The histogram of elevation change for glaciers within the circle (derived from HMA-3). (h) The histogram of the differences between glacier elevation changes derived from the HMA-2 and HMA-4, i.e., c−a, and f−d.

We provide DEM co-registration examples in the Supplement for more scenarios in the HMA and New Zealand (NZL), such as a large number of glaciers, a large amount of vegetation, a high noise level due to rough topography in the DEMs, etc. Since no strong jitter-induced residuals were observed in the co-registration results of these DEM pairs, residual correction experiments were not performed.

5. Discussion

The performance of different types of DEM co-registration methods has been intensively investigated by Paul et al. (2015) and Vacaflor et al. (2022). Their tests showed that the method of Nuth and Kääb achieved similar or better accuracy compared to the grid search method (Paul et al., 2015), the LS3D method (Paul et al., 2015), and the subwatershed-based method (Vacaflor et al., 2022), and it was recommended for practical applications due to the less computational effort (Paul et al., 2015). This paper focuses on the analytical (i.e., the terrain information based) methods only. Our theoretical analysis indicates that the method of Rosenholm and Torlegard can be regarded as an extension of the method of Nuth and Kääb by additionally modeling the scale and rotation errors. As both the two algorithms can be expressed in a linear form, the method of Rosenholm and Torlegard retains all the advantages of the method of Nuth and Kääb. The DEM co-registration algorithm used in Noh and Howat (2014) is also an analytical solution, but it employs a nonlinear model with a very complicated form, which is not intuitive for non-experts. Given that it is theoretically compatible with the method of Rosenholm and Torlegard, the algorithm of Noh and Howat was not included in our comparative experiments.

It is well known that extrapolation often leads to unreliable results. Figure 10 shows an example of residual regression by taking the terrain elevation as the explanatory variable. It can be seen from Fig. 10a that both the prediction results of the polynomial and spline fitting methods are strongly biased in high altitude regions (> 500 m). As the mean elevation of glaciers is often much higher than that of bare lands (e.g., Fig. 10b), a long extrapolation is frequently required in cryosphere studies. A solution for the problem is to decrease the degree-of-freedom of the regression model, e.g., reducing the degree of the polynomial (in high-order polynomial regression) or smoothing (in spline regression), and dropping some explanatory variables (in DEM co-registration). Given that obvious elevation-dependent biases were not observed in our experiments (e.g., Fig. 10a), the terrain elevation was not introduced as an explanatory variable in the residual regression (i.e., its degree-of-freedom is zero). The extrapolation issue also occurs when bare lands are very unevenly distributed geographically in the overlapping region of a DEM pair. In this particular case, the performance of all the methods in Sects. 2 and 3 (i.e., the DEM co-registration methods and residual regression methods for the along-track and cross-track directions) varies greatly with different scenarios, and it is impossible to draw any definite conclusions from the comparative experiments. A rule of thumb is to choose a simple regression model first, and then to try some more accurate but possibly unstable methods.

In the last section, only DEM pairs with good geometric conditions were tested. For the DEM pairs located at the edge of Ice Sheet or covered by heavy clouds, the geometric constraint of stable terrain may be very weak, and a long extrapolation is sometimes required. Figure 12 shows a representative example of one ASTER DEM pair located on the western edge of GrIS, where the stable terrain is geographically distributed in the southwest corner only. The time interval between reference DEM (ASTER DEM 20190725) and secondary DEM (ASTER DEM 20190826) is one month, and therefore the ice surface elevation can be considered unchanged. Although the Rosenholm and Torlegard algorithm yields significantly smaller co-registration residuals in the stable region than the Nuth and Kääb method, it is prone to producing larger biases over ice-covered regions. These biases cannot be removed by residual correction procedure, because the residual trend over ice-covered regions is completely different from that over stable regions.

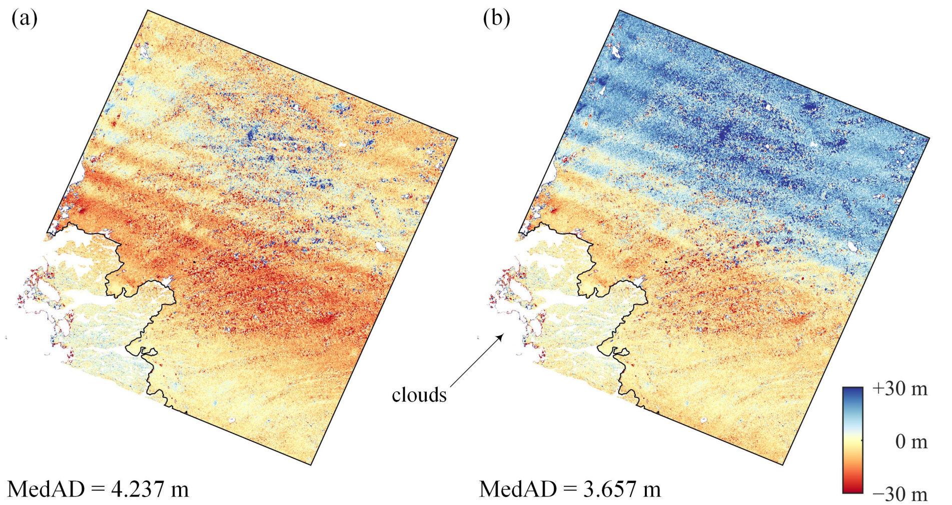

Figure 12. Co-registration results of ASTER DEM 20190725 (Scene ID: AST14DEM.003:2344943025) and ASTER DEM 20190826 (Scene ID: AST14DEM.003:2346334895). (a) The linear versions of the method of Nuth and Kääb. (b) The method of Rosenholm and Torlegard.

The data extrapolation issue often occurs in residual correction along terrain heights. As the mean elevation of glaciers is often much higher than that of bare lands, a long extrapolation is frequently required. Figure 13 shows an example of residual regression by taking the terrain elevation as the explanatory variable (DEM pair GrIS-19 in Table S1). Both the prediction results of the polynomial and spline fitting methods are strongly biased in high altitude regions (> 500 m).

A solution for the extrapolation problem is to decrease the degree-of-freedom of the regression model, e.g., dropping some explanatory variables (in DEM co-registration), and reducing the degree of the polynomial (in high-order polynomial regression) or smoothing (in spline regression). Given that obvious elevation-dependent biases were not observed in our experiments (e.g., Fig. 13a), the terrain elevation was not introduced as an explanatory variable in our residual regression model (i.e., its degree-of-freedom is zero).

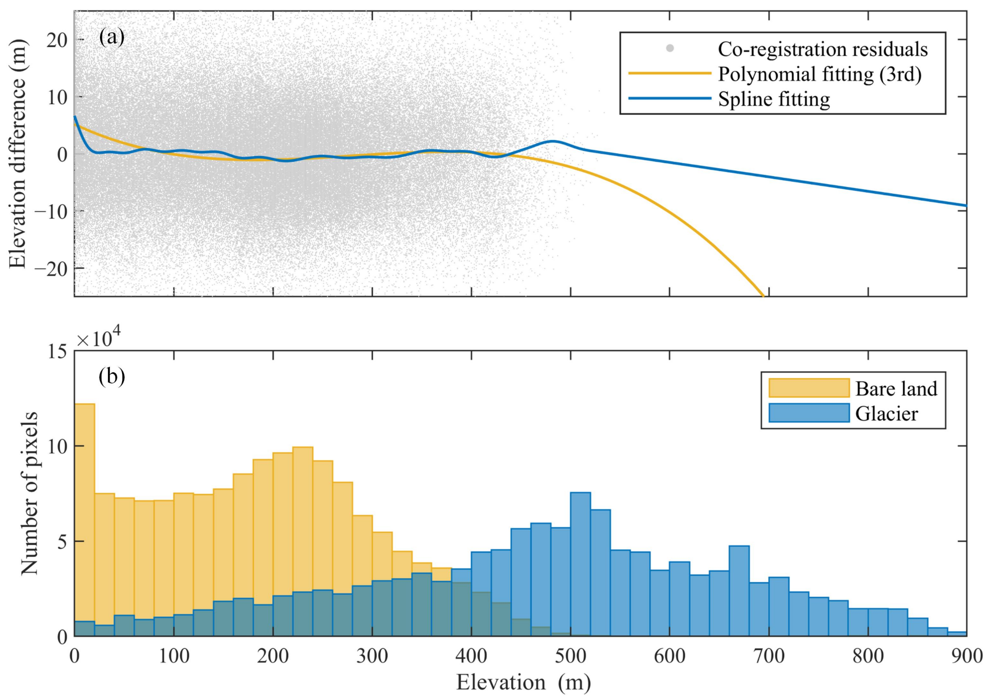

Figure ~~10~~13. Regressions of DEM co-registration residuals against terrain heights. (a) Polynomial and spline fitting results. (b) The histograms of terrain heights for bare land and glacier covered pixels in the overlapping region of ~~a~~ DEM pair GrIS-19.

6. Conclusion

In this paper, we have made a thorough comparison of the DEM co-registration methods of Nuth and Kääb and Rosenholm and Torlegard, and proposed a GAM-based method to correct DEM co-registration residuals. The theoretical analysis and experimental results support the following conclusions:

1) There are only some negligible differences between the original versions of the method of Nuth and Kääb and the method of Rosenholm and Torlegard. On the one hand, the terrain-related information used by Nuth and Kääb (2011) and Rosenholm and Torlegard (1988) as explanatory variables in their regressions—slope/aspect and gradient—can be proven to be equivalent through theoretical analysis. On the other hand, even though the method of Nuth and Kääb and the method of Rosenholm and Torlegard utilize distinct regression forms, the nonlinear regression equation used by the former can be converted into a linear equation with the same structure as the latter.

2) Rotation and scale biases should be taken into account in DEM co-registration. The only significant difference between the method of Nuth and Kääb and the method of Rosenholm and Torlegard is that the latter models the translation, scale, and rotation-induced biases, while the former only considers the spatial translation. Comparative experiments conducted

on ~~23 ASTER~~ multiple DEM pairs showed that the method of Rosenholm and Torlegard consistently outperformed the method of Nuth and Kääb in terms of co-registration residuals.

3) GAM spline fitting can be used as an alternative to traditional parametric regression models in correcting DEM co-registration residuals. ASTER DEMs often suffer from some complex errors with multiple frequencies induced by satellite attitude jitter. Benefiting from its data-driven nature, the GAM spline fitting method can capture the complex nonlinear patterns in DEM co-registration residuals, whereas the performance of the parametric regression methods is sometimes limited by their predefined models.

Data availability. ASTER DEMs are freely available at https://search.earthdata.nasa.gov. Landsat 8 images are available at https://glovis.usgs.gov.

Supplement. The supplement related to this article is available online at:

Author contributions. XS and TL conceptualized and initiated the study. TL performed the data processing and analyses, prepared the figures and tables, and wrote the draft manuscript. XS contributed to review and improve the manuscript. YH, BL, LJ, and HW assisted to the editing and refining of the manuscript.

Competing interests. The authors declare that they have no conflict of interest.

Financial support. This research was supported by the National Key R & D Program of China (Nos. 2017YFA0603103 and 2018YFC1406102); the Strategic Priority Research Program of the Chinese Academy of Sciences (No. XDA19070104); the National Natural Science Foundation of China (Nos. 41974009, 42004007 and 42174046); the State Key Laboratory of Geodesy and Earth's Dynamics (Innovation Academy for Precision Measurement Science and Technology, CAS, Nos. S21L6102 and S22L6101); and the Key Research Program of Frontier Sciences, CAS (Nos. QYZDB-SSW-DQC042 and QYZDJ-SSW-DQC027).

References

Aguilar, F. J., Aguilar, M. A., Fernandez, I., Negreiros, J. G., Delgado, J., and Perez, J. L.: A New Two-Step Robust Surface Matching Approach for Three-Dimensional Georeferencing of Historical Digital Elevation Models, IEEE Geosci. Remote Sens. Lett., 9, 589–593, https://doi.org/10.1109/LGRS.2011.2175899, 2012.

AIRBUS: Copernicus DEM: Copernicus digital elevation model product handbook, Report AO/1-9422/18/I-LG, 2020.

Akca, D.: Co-registration of Surfaces by 3D Least Squares Matching, Photogramm. Eng. Remote Sens., 76, 307–318, https://doi.org/10.14358/PERS.76.3.307, 2010.

Badekas, J.: Investigations related to the establishment of a World Geodetic System. The Ohio State University Columbus Dept of Geodetic Science, Columbus, Ohio State, USA, 1969.

Berthier, E., Cabot, V., Vincent, C., and Six, D.: Decadal Region-Wide and Glacier-Wide Mass Balances Derived from Multi-Temporal ASTER Satellite Digital Elevation Models. Validation over the Mont-Blanc Area, Front. Earth Sci., 4, 63, https://doi.org/10.3389/feart.2016.00063, 2016.

Berthier, E., Arnaud, Y., Kumar, R., Ahmad, S., Wagnon, P., and Chevallier, P.: Remote sensing estimates of glacier mass balances in the Himachal Pradesh (Western Himalaya, India), Remote Sens. Environ., 108, 327–338, https://doi.org/10.1016/j.rse.2006.11.017, 2007.

Besl, P. J. and Mckay, N. D.: A Method for Registration of 3-D Shapes, IEEE Trans. Pattern Anal. Mach. Intell., 14, 239–256, https://doi.org/10.1109/34.121791, 1992.

Bolch, T., Pieczonka, T., and Benn, D. I.: Multi-decadal mass loss of glaciers in the Everest area (Nepal Himalaya) derived from stereo imagery, The Cryosphere, 5, 349–358, https://doi.org/10.5194/tc-5-349-2011, 2011.

Brun, F., Berthier, E., Wagnon, P., Kääb, A., and Treichler, D.: A spatially resolved estimate of High Mountain Asia glacier mass balances from 2000 to 2016, Nat. Geosci., 10, 668–673, https://doi.org/10.1038/ngeo2999, 2017.

Cucchiaro, S., Maset, E., Cavalli, M., Crema, S., Marchi, L., Beinat, A., and Cazorzi, F.: How does co-registration affect geomorphic change estimates in multi-temporal surveys?, GISci. Remote Sens., 57, 611–632, https://doi.org/10.1080/15481603.2020.1763048, 2020.

Di, K., Hu, W., Liu, Y., and Peng, M.: Co-registration of Chang'E-1 stereo images and laser altimeter data with crossover adjustment and image sensor model refinement, Adv. Space Res., 50, 1615–1628, https://doi.org/10.1016/j.asr.2012.06.037, 2012.

Farr, T. G., Rosen, P. A., Caro, E., Crippen, R., Duren, R., Hensley, S., Kobrick, M., Paller, M., Rodriguez, E., Roth, L., Seal, D., Shaffer, S., Shimada, J., Umland, J., Werner, M., Oskin, M., Burbank, D., and Alsdorf, D.: The Shuttle Radar Topography Mission, Rev. Geophys., 45, RG2004, https://doi.org/10.1029/2005RG000183, 2007.

Gardelle, J., Berthier, E., Arnaud, Y., and Kääb, A.: Region-wide glacier mass balances over the Pamir-Karakoram-Himalaya during 1999–2011, The Cryosphere, 7, 1263–1286, https://doi.org/10.5194/tc-7-1263-2013, 2013.

Girod, L., Nuth, C., Kääb, A., McNabb, R., and Galland, O.: MMASTER: Improved ASTER DEMs for Elevation Change Monitoring, Remote Sens., 9, 704, https://doi.org/10.3390/rs9070704, 2017.

Gorokhovich, Y. and Voustianiouk, A.: Accuracy assessment of the processed SRTM-based elevation data by CGIAR using field data from USA and Thailand and its relation to the terrain characteristics, Remote Sens. Environ., 104, 409–415, https://doi.org/10.1016/j.rse.2006.05.012, 2006.

Gruen, A. and Akca, D.: Least squares 3D surface and curve matching, ISPRS-J. Photogramm. Remote Sens., 59, 151–174, https://doi.org/10.1016/j.isprsjprs.2005.02.006, 2005.

Hastie, T. and Tibshirani, R.: Generalized additive models. Chapman and Hall, London, 1990.

Hofton, M., Dubayah, R., Blair, J. B., and Rabine, D.: Validation of SRTM elevations over vegetated and non-vegetated terrain using medium footprint lidar, Photogramm. Eng. Remote Sens., 72, 279–285, https://doi.org/10.14358/PERS.72.3.279, 2006.

Jun, C., Ban, Y., and Li, S.: Open access to Earth land-cover map, Nature, 514, 434, https://doi.org/10.1038/514434c, 2014.

Karkee, M., Steward, B. L., and Aziz, S. A.: Improving quality of public domain digital elevation models through data fusion, Biosyst. Eng., 101, 293–305, https://doi.org/10.1016/j.biosystemseng.2008.09.010, 2008.

~~Ke, L., Song, C., Wang, J., Sheng, Y., Ding, X., Yong, B., Ma, R., Liu, K., Zhan, P., and Luo, S.: Constraining the contribution of glacier mass balance to the Tibetan lake growth in the early 21st century, Remote Sens. Environ., 268, 112779, https://doi.org/10.1016/j.rse.2021.112779, 2022.~~

Leprince, S., Ayoub, F., Klinger, Y., and Avouac, J.: Co-Registration of Optically Sensed Images and Correlation (COSI-Corr): an operational methodology for ground deformation measurements, 2007 IEEE International Geoscience and Remote Sensing Symposium, Barcelona, Spain, 23–28 July 2007, 1943–1946, https://doi.org/10.1109/IGARSS.2007.4423207, 2007.

Li, C., Jiang, L., Liu, L., and Wang, H.: Regional and Altitude-Dependent Estimate of the SRTM C/X-Band Radar Penetration Difference on High Mountain Asia Glaciers, IEEE J. Sel. Top. Appl. Earth Observ. Remote Sens., 14, 4244–4253, https://doi.org/10.1109/jstars.2021.3070362, 2021.

Li, H., Deng, Q. L., and Wang, L. C.: Automatic Co-Registration of Digital Elevation Models Based on Centroids of Subwatersheds, IEEE Trans. Geosci. Remote Sensing, 55, 6639–6650, https://doi.org/10.1109/Tgrs.2017.2731048, 2017.

~~Lin, H., Li, G., Cuo, L., Hooper, A., and Ye, Q.: A decreasing glacier mass balance gradient from the edge of the Upper Tarim Basin to the Karakoram during 2000–2014, Sci Rep, 7,6712 (2017) https://doi.org/10.1038/s41598-017-07133-8, 2017.~~

Liu, L., Jiang, L., Jiang, H., Wang, H., Ma, N., and Xu, H.: Accelerated glacier mass loss (2011–2016) over the Puruogangri ice field in the inner Tibetan Plateau revealed by bistatic InSAR measurements, Remote Sens. Environ., 231, 111241, https://doi.org/10.1016/j.rse.2019.111241, 2019.

Liu, L., Jiang, L., Zhang, Z., Wang, H., and Ding, X.: Recent Accelerating Glacier Mass Loss of the Geladandong Mountain, Inner Tibetan Plateau, Estimated from ZiYuan-3 and TanDEM-X Measurements, Remote Sens., 12, 472, https://doi.org/10.3390/rs12030472, 2020.

McMillan, M., Muir, A., Shepherd, A., Escola, R., Roca, M., Aublanc, J., Thibaut, P., Restano, M., Ambrozio, A., and Benveniste, J.: Sentinel-3 Delay-Doppler altimetry over Antarctica, The Cryosphere, 13, 709–722, https://doi.org/10.5194/tc-13-709-2019, 2019.

Molodenskii, M.S.: Methods for study of the external gravitational field and figure of the Earth, Jerusalem, 1962.

NASA, METI, AIST, Japan Spacesystems and U.S./Japan ASTER Science Team.: ASTER DEM Product, NASA EOSDIS Land Processes DAAC [data set], https://doi.org/10.5067/ASTER/AST14DEM.003, 2001.

Nguyen, C. T., Chidthaisong, A., Kieu Diem, P., and Huo, L.-Z.: A Modified Bare Soil Index to Identify Bare Land Features during Agricultural Fallow-Period in Southeast Asia Using Landsat 8, Land, 10, 231, https://doi.org/10.3390/land10030231, 2021.

Noh, M. and Howat, I. M.: Automated Coregistration of Repeat Digital Elevation Models for Surface Elevation Change Measurement Using Geometric Constraints, IEEE Trans. Geosci. Remote Sensing, 52, 2247–2260, https://doi.org/10.1109/TGRS.2013.2258928, 2014.

Nuth, C. and Kääb, A.: Co-registration and bias corrections of satellite elevation data sets for quantifying glacier thickness change, The Cryosphere, 5, 271–290, https://doi.org/10.5194/tc-5-271-2011, 2011.

Paul, F., Bolch, T., Kääb, A., Nagler, T., Nuth, C., Scharrer, K., Shepherd, A., Strozzi, T., Ticconi, F., Bhambri, R., Berthier, E., Bevan, S., Gourmelen, N., Heid, T., Jeong, S., Kunz, M., Lauknes, T. R., Luckman, A., Merryman Boncori, J. P., Moholdt, G., Muir, A., Neelmeijer, J., Rankl, M., VanLooy, J., and Van Niel, T.: The glaciers climate change initiative: Methods for creating glacier area, elevation change and velocity products, Remote Sens. Environ., 162, 408–426, https://doi.org/10.1016/j.rse.2013.07.043, 2015.

Peckham, R. J. and Jordan, G.: Digital Terrain Modelling: Development and Applications in a Policy Support Environment, Springer Berlin, Heidelberg, https://doi.org/10.1007/978-3-540-36731-4, 2007.

Peduzzi, P., Herold, C., and Silverio, W.: Assessing high altitude glacier thickness, volume and area changes using field, GIS and remote sensing techniques: the case of Nevado Coropuna (Peru), The Cryosphere, 4, 313–323, https://doi.org/10.5194/tc-4-313-2010, 2010.

Pieczonka, T., Bolch, T., Junfeng, W., and Shiyin, L.: Heterogeneous mass loss of glaciers in the Aksu-Tarim Catchment (Central Tien Shan) revealed by 1976 KH-9 Hexagon and 2009 SPOT-5 stereo imagery, Remote Sens. Environ., 130, 233–244, https://doi.org/10.1016/j.rse.2012.11.020, 2013.

Rodriguez, E., Morris, C. S., and Belz, J. E.: A global assessment of the SRTM performance, Photogramm. Eng. Remote Sens., 72, 249–260, https://doi.org/10.14358/Pers.72.3.249, 2006.

Rosenholm, D. and Torlegard, K.: Three-dimensional absolute orientation of stereo models using digital elevation models, Photogramm. Eng. Remote Sens., 54, 1385–1389, 1988.

Rusinkiewicz, S. and Levoy, M.: Efficient variants of the ICP algorithm, Proceedings third international conference on 3-D digital imaging and modeling, Quebec City, Canada, 28 May – 1 June 2001,145–152, https://doi.org/10.1109/IM.2001.924423, 2001.

Sedaghat, A. and Naeini, A. A.: DEM orientation based on local feature correspondence with global DEMs, GISci. Remote Sens., 55, 110–129, https://doi.org/10.1080/15481603.2017.1364879, 2018.

Tang, X., Yue, Q., and Gao, X.: China DSM Generation and Accuracy Acessment Using ZY3 Images, in: Proceedings of the IEEE International Geoscience and Remote Sensing Symposium, Valencia, Spain, 23–27 July 2018, 6757-6760, 2018.

Trevisani, S. and Rocca, M.: MAD: robust image texture analysis for applications in high resolution geomorphometry, Comput. Geosci., 81, 78–92, https://doi.org/10.1016/j.cageo.2015.04.003, 2015.

Vacaflor, P., Lenzano, M. G., Vich, A., and Lenzano, L.: Co-Registration Methods and Error Analysis for Four Decades (1979–2018) of Glacier Elevation Changes in the Southern Patagonian Icefield, Remote Sens., 14(4), 820, https://doi.org/10.3390/rs14040820, 2022.

Van Niel, T. G., McVicar, T. R., Li, L. T., Gallant, J. C., and Yang, Q. K.: The impact of misregistration on SRTM and DEM image differences, Remote Sens. Environ., 112, 2430–2442, https://doi.org/10.1016/j.rse.2007.11.003, 2008.

Wood, S. N.: Mixed GAM Computation Vehicle with Automatic Smoothness Estimation, R package 'mgcv', version 1.8-40 [code], 2022.

Wood, S. N.: Generalized Additive Models: An Introduction with R, Second Edition, Texts in Statistical Science, Chapman & Hall/CRC, https://doi.org/10.1201/9781315370279, 2017.

Wu, B., Guo, J., Hu, H., Li, Z. L., and Chen, Y. Q.: Co-registration of lunar topographic models derived from Chang'E-1, SELENE, and LRO laser altimeter data based on a novel surface matching method, Earth Planet. Sci. Lett., 364, 68–84, https://doi.org/10.1016/j.epsl.2012.12.024, 2013.

Zhang, T., Lei, B., Wang, J., Li, Y., Liu, K., and Li, T.: Preliminary Quality Analysis of the Triple Linear-Array and Mul Tispectral Images of ZY-3 02 Satellite, in: Proceedings of the IEEE International Geoscience and Remote Sensing Symposium, Valencia, Spain, 23–27 July 2018, 9172-9175, 2018.